Accretion Dynamics on Wet Granular Materials

Guillaume Saingier, Alban Sauret, Pierre Jop

Accretion Dynamics on Wet Granular Materials

Guillaume Saingier, Alban Sauret, and Pierre Jop
Surface du Verre et Interfaces, UMR 125, CNRS/Saint-Gobain, 39, quai Lucien Lefranc, F-93303 Aubervilliers, Cedex France

Wet granular aggregates are common precursors of construction materials, food, and health care products. The physical mechanisms involved in the mixing of dry grains with a wet substrate are not well understood and difficult to control. Here, we study experimentally the accretion of dry grains on a wet granular substrate by measuring the growth dynamics of the wet aggregate. We show that this aggregate is fully saturated and its cohesion is ensured by the capillary depression at the air-liquid interface. The growth dynamics is controlled by the liquid fraction at the surface of the aggregate and exhibits two regimes. In the viscous regime, the growth dynamics is limited by the capillary-driven flow of liquid through the granular packing to the surface of the aggregate. In the capture regime, the capture probability depends on the availability of the liquid at the saturated interface, which is controlled by the hydrostatic depression in the material. We propose a model that rationalizes our observations and captures both dynamics based on the evolution of the capture probability with the hydrostatic depression.

Wet granular materials are common precursors of construction materials, food and health care products as well as relevant in many geophysical processes [1]. Indeed, the addition of liquid drastically modifies the behavior of a granular medium, and its rheological properties strongly depend on the proportion of the liquid [1–3]. For large liquid volume fractions, a dense suspension is produced exhibiting fluidlike properties [4, 5]. By contrast, the presence of small amounts of liquid induces the formation of liquid bridges between grains, providing a strong cohesion to the material and a solidlike behavior [1, 6–10]. These effects are commonly used in civil engineering processes that require mixing dry grains with a liquid to obtain new physical or chemical properties. Although the final product is homogeneous at the large scale, strong spatial heterogeneities in the liquid content are present during the blending, with rheological properties ranging from a dry state to a suspension in the mixture. Understanding how dry grains are incorporated into wet granular substrates thus requires coupling the dynamical interplay between the grains and the liquid. Most studies on the granulation in powders [11] consider the final size distribution of the aggregates. Other studies focus either on a static granular material, described as a porous medium, in contact with a fluid reservoir [12–15], or on the global rheological response during the blending process [16]. Only recently, some studies have considered the coupling between liquid and moving grains. For a low liquid content, the dry granular flow erodes the wet cohesive grains [17, 18], whereas for a large liquid content, a stable and cohesive structure is built by accretion of dry grains on the wet granular phase [19]. However, the local mechanisms and the accretion dynamics of dry grains onto a wet granular substrate are not well understood.

In this Letter, we investigate experimentally the accretion process between a static wet granular material and flowing grains using a model experiment presented schematically in Fig. 1. The accretion process results in the growth of the wet aggregate on a horizontal substrate. At the beginning of the experiment, the static wet granular substrate is made of spherical glass beads of diameter $d_g = 315$-355 μm prepared in a vertical tube [Fig. 1(a)] with a height $h_g = 10$ mm and a diameter equal to 10 mm. To keep the beads wet with a fixed hydrostatic pressure in the interstitial fluid, this substrate is connected to a water reservoir with an adjustable level through a porous membrane. We note Δh the distance between the top of the substrate and the water level. The substrate is fully saturated, and the capillary pressure drop associated to the local curvature of the menisci balances the hydrostatic depression at the liquid- air interface:

$$p_0 - \frac{2\gamma\cos\theta}{R} = p_0 - \rho g \Delta h, \tag{1}$$

where p_0 is the atmospheric pressure, $\gamma = 71$ mN/m ($\pm$ 1 mN/m) the surface tension of the water, $\rho = 1$ g/cm^3 the water density, $\theta = 27°$ ($\pm$ 5°) the contact angle of the water on a glass bead [20] and $1/R$ the mean curvature of the meniscus at the interface.

To study the accretion, identical dry glass beads are poured on the wet substrate at constant flow rate $Q_g = 1.1$ g/s using an inox funnel of diameter 3 mm connected to a 20-cm-long and 6 mm diameter inox tubing with a flexible end. A grid is placed between the funnel and the tube to disperse the grains and create a diluted jet collimated by the tube. The grains are ejected with an angle of about 45° with the horizontal at constant velocity ($v_g \simeq 1.6$ m/s) controlled, in the diluted regime, by the length of the tube. As the aggregate grows by the accretion of dry grains, the funnel is moved away at the growth velocity, so that the grains are released at a constant distance from the wet substrate, typically 5 mm. Note that the accretion occurs on a horizontal plane, so the hydrostatic depression in the interstitial liquid remains constant during an experiment. A thin PMMA plate of width 6 mm is used to support the weight of the

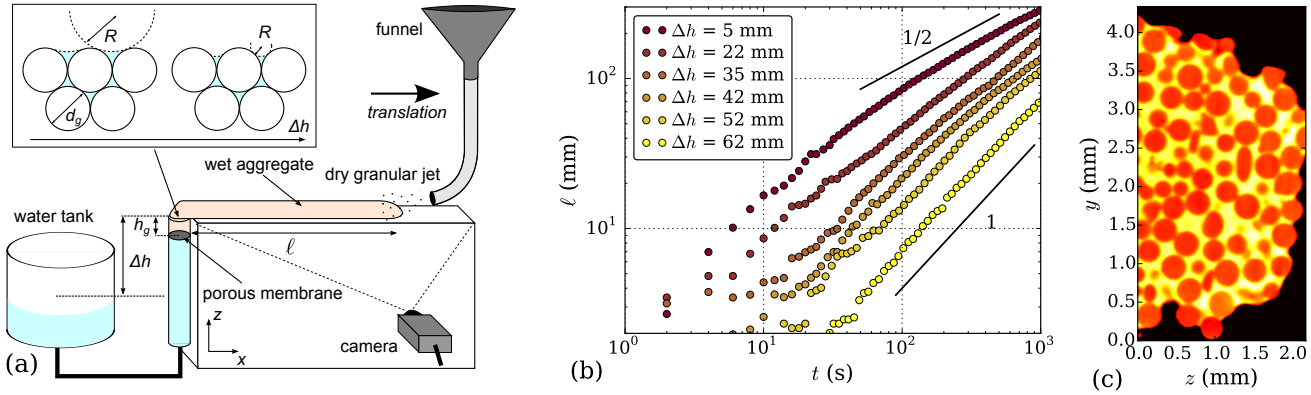

FIG. 1. (a) Schematic of the experimental set-up. Inset: Schematic of the meniscus for increasing Δh. (b) Time evolution of the length of the aggregate for different hydrostatic depressions, expressed as a function of Δh. (c) Cross section through a 3D tomogram of a wet aggregate. The liquid is colored in yellow whereas the glass beads are red and the air is in black.

aggregate during its growth and avoid the accumulation of grains that are not trapped, which bounce off after the impact. PMMA is chosen as it is less hydrophilic than the glass beads and does not influence the growth dynamics [21]. The growth of the aggregate is recorded at 0.5 Hz with a CCD camera and analyzed by image processing.

We investigate the role of the hydrostatic depression by performing systematic experiments at different water heights in the tank, Δh. The growth dynamics is reported in Fig. 1(b), where we plot the length of the aggregate ℓ as a function of time for a constant Q_g and v_g. The growth rate decreases when Δh increases, indicating that the accretion process is less efficient for a large hydrostatic depression. Moreover, the dynamics drastically evolves with Δh and exhibits a smooth transition from a diffusive regime at low Δh, where ℓ is proportional to $t^{1/2}$, and a linear regime at large Δh, where ℓ is proportional to t [Fig. 1(b)]. To understand how the liquid is distributed in the aggregate during the accretion process, we image the microstructure with X-ray tomography [10, 21]. The 3D reconstruction shows that the aggregate is fully saturated without any air bubble for any value of Δh [Fig. 1(c)]. The aggregate is in a capillary state and the cohesion of the structure results from the capillary depression at the air/liquid interface [8]. Therefore, during an experiment, the curvatures of the menisci are in equilibrium with the local pressure along the wet aggregate.

To understand the existence of these two different regimes, we propose a local growth mechanism by granular accretion. The aggregate growth is directly related to the fraction of dry grains captured at the liquid interface of the wet material. As dry grains are added, the liquid has to penetrate into the granular packing to reach its equilibrium position and to be accessible to the impacting granular jet. At low hydrostatic depression (small Δh) [inset of Fig. 1(a)], the air/liquid interface is slightly curved and easily available to capture a large fraction of impacting grains. In this case, the growth dynamics is limited by the viscous displacement of the fluid into the granular packing. This viscous regime is modeled by the Darcy's law connecting the flow velocity to the driving pressure corresponding here to the capillary pressure in the pores. The Lucas-Washburn equation describes the imbibition in all the granular structure of total length L^v, which is the sum of the aggregate length ℓ^v and the substrate length h_g [23]:

$$L^v(t) = \ell^v(t) + h_g = \sqrt{\frac{2k\Delta p}{\eta}(t + t_0)}, \qquad (2)$$

where k is the permeability of the packing, η is the dynamic viscosity of the fluid, t_0 is the time for the liquid to penetrate into the substrate and $\Delta p = p_c - \rho g \Delta h$ the capillary pressure reduced by the hydrostatic depression. The pressure p_c is associated to the pore radius r_p and defined as $2\gamma\cos\theta/r_p$. In the following, r_p is taken equal to the grain radius $d_g/2$ [13]. Note that t_0 is equal to ${h_g}^2\eta/2k\Delta p^{h_g}$, where $\Delta p^{h_g} = p_c - \rho g(\Delta h - h_g)$. In the range of height Δh investigated, t_0 varies between 0.7 s and 3 s and will be neglected in the following as it remains small compared to the time scale of our experiments. In this regime, the aggregate length scales as $t^{1/2}$ in agreement with the experimental results.

A second regime is explored at large Δh corresponding to large hydrostatic depressions. In this situation the menisci are strongly deformed and the liquid is less accessible to the impacting grains. The growth dynamics of the aggregate is then limited by the efficiency of the capture process. Consequently, the growth rate can be defined using the fraction of grains captured over the amount of grains impacting the aggregate. Introducing the capture probability $\mathcal{P}_{capt}$ and assuming that this probability is constant during an experiment, where Δh remains constant, the growth dynamics in the capture

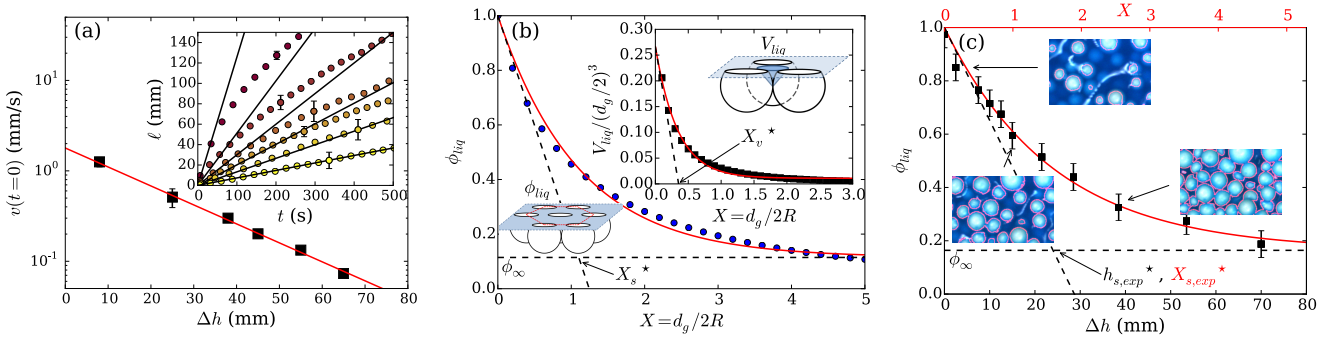

FIG. 2. (a) Initial growth rate of the aggregate $v(t=0)$ as a function of the height Δh. The fit gives $h^\star = 20$ mm ($X^\star = 0.26$). Inset: Temporal evolution of the aggregate length. (b) Evolution of the liquid fraction ϕ_{liq} at the liquid/air interface in a wet granular packing as the function of the ratio $X = 2d_g/R$. Data are fitted by $\phi_{liq} = \phi_\infty + (1-\phi_\infty)\exp(-X/X_s^\star)$ with $X_s^\star = 1.10$. Inset: Evolution of the dimensionless volume associated to a conical site of capture - $X_v^\star = 0.34$. (c) Experimental evolution of the apparent liquid surface as function of height Δh. Images are obtained by binocular microscopy with an opaque dyed liquid and zirconium beads of 500 μm diameter. The red line is an exponential expression with $h_{s,exp}^\star = 24$ mm $\pm$ 4 mm corresponding to $X_{s,exp}^\star = 1.59 \pm 0.26$. Experimental parameters: $\gamma = 44$ mN/m ($\pm$ 2 mN/m), $\theta = 65^\circ$ ($\pm$ 5°)]

.

regime is:

$$\ell^c(t) = \frac{Q_g}{\rho_s \phi S}\,\mathcal{P}_{capt}\,t, \tag{3}$$

where $\rho_s = 2.5$ g/cm^3 is the grain density, $\phi = 0.63 \pm 0.01$ is the compacity of the aggregate and S its cross-section.

The transition from the viscous regime to the capture regime occurs when the typical growth rates associated to those two limiting mechanisms are comparable. Equating the growth rates leads to a typical time scale t_c and a typical length scale ℓ_c characterizing the growth process. These parameters depend on the capture probability and are defined as:

$$t_c = \frac{k}{2\eta}\left(\frac{\rho_g \phi S}{\mathcal{P}_{capt} Q_g}\right)^2 \Delta p, \quad \ell_c = \frac{k}{2\eta}\frac{\rho_g \phi S}{\mathcal{P}_{capt} Q_g}\Delta p. \tag{4}$$

Moreover, our experiments show that the capture probability $\mathcal{P}_{capt}$ decreases with the height Δh, thus with the hydrostatic depression. To estimate this variation, we compute the initial growth velocity $v(t=0)$ for each experiment. At the beginning of the growth, the accretion process is not limited by the rate of imbibition through the short porous aggregate, but only by the capture rate of the first grains. As shown in Fig. 2(a), the initial growth rate decreases exponentially with the altitude Δh and the variation of the capture probability reads:

$$v(\Delta h, t=0) = v_0 \exp\left(-\frac{\Delta h}{h^\star}\right) = \frac{Q_g}{\rho_s \phi S}\mathcal{P}_{capt}(\Delta h), \tag{5}$$

thus,

$$\mathcal{P}_{capt}(\Delta h) = \mathcal{P}_0 \exp\left(-\frac{\Delta h}{h^\star}\right), \tag{6}$$

where $h^\star = 20$ mm is the length characterizing the velocity decrease and $\mathcal{P}_0 = (\rho_s \phi S v_0)/Q_g$ is the capture probability at the water level with $v_0 = 1.86$ mm/s. A similar expression was found empirically for the rising velocity of a vertical granular tower [19]. We defined the dimensionless curvature $X = d_g/2R$ which is related to the height Δh by Eq. (1) such that $X = (d_g \rho g/\gamma\cos\theta)\Delta h$, which gives the dimensionless length associated to the velocity decrease, $X^\star = (d_g \rho g/\gamma\cos\theta)\,h^\star = 0.26$.

To explain the expression of the probability, we propose a crude geometrical model that relates on the liquid distribution at the air/liquid interface with the probability to capture a grain. As the aggregate is fully saturated, the hydrostatic depression, associated with Δh, retracts the liquid menisci. Thus the interfacial liquid area and volume decrease. We first approximate the air/liquid interface by a plane located at the bottom of a spherical meniscus and intersecting a dense layer of spheres (see the schematics of Fig. 2(b) and [21] for details of the calculation). Furthermore, we assume that the liquid is perfectly wetting the beads which are organized in a hexagonal lattice [21]. Under these assumptions, we calculate the liquid area as a function of X [Fig 2(b)]. In addition, we report the liquid volume calculated using the cone inscribed between the spheres [inset of Fig 2(b)] [21]. Both the evolution of the area and the volume are fitted by an exponential decay in agreement with the expression proposed for the capture probability. We define $X_s^\star$ and $X_v^\star$ as the characteristic dimensionless length associated to each decay, respectively [Fig. 2(b)]. Fitting the numerical data leads to $X_s^\star = 1.10$ and $X_v^\star = 0.34$. The value of $X_v^\star$, compared to $X^\star$, suggests that the capture probability depends on the volume of liquid available between the interfacial grains. Furthermore, the evolution of the liquid distribution is obtained by direct imaging of the liquid at the interface of a wet granular material for varying Δh [see Fig. 2(c) and [21] for experimental details]. An exponential decrease is ob-

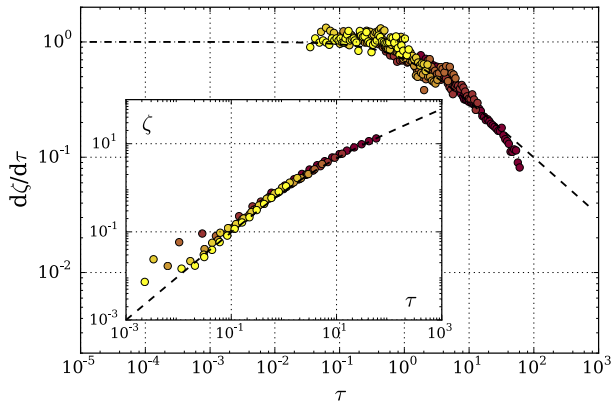

FIG. 3. Evolution of the rescaled growth velocity $d\zeta/d\tau$ as a function of the rescaled time τ defined in Eq. 4 for all hydrostatic depressions. Inset: Evolution of the rescaled length of aggregate ζ as the function of the rescaled time τ. The dashed lines correspond to the theoretical predictions given by Eq. (8).

served with $X_{s,exp}{}^{\star} = 1.59 \pm 0.26$, consistent with the computed value. Using the values of v_0 and $h^{\star}$ determined experimentally, we compute the length ℓ_c and the time t_c and introduce the rescaled parameters $\zeta = \ell/\ell_c$ and $\tau = t/t_c$. The rescaled data are plotted in Fig. 3 for different heights [21]. The data collapse well on a master curve, confirming that the aggregate growth is dominated by the competition between the sticking properties of the grains and the properties of the flow in a porous medium. Our model based on the menisci retraction as well as our tomographic reconstructions show that air bubbles are not present in the aggregate as suggested by Pacheco *et al.* who claim that granular towers can emerge both in funicular and capillary states. Their argument was developed to explain their measurements of an apparent exponential decrease of the ratio between the mass of liquid and the mass of grains along a vertical granular tower [19]. Our results demonstrates that the accretion is an interfacial phenomenon, which only takes place in the capillary state. Finally, our model also provides an explanation for the logarithmic rise dynamics recorded for vertical towers, which takes place in the capture regime.

To predict the full accretion dynamics and the smooth transition between the two regimes, we introduce two characteristic times. Indeed, to increase the length ℓ of the aggregate by one grain diameter d_g, we can separate the process into a capture time τ_{capt} associated to the capture process followed by a viscous time τ_{visc} corresponding to the fluid motion in the last layer of grains until the equilibrium position of the meniscus is reached. These times are estimated using the growth rate associated to each phenomenon (see Eqs. 2 and 3):

$$\tau_{capt} = \frac{d_g \rho_g \phi S}{Q_g \mathcal{P}_{capt}}, \quad \tau_{visc} = \frac{\eta}{k}\frac{\ell d_g}{\Delta p}. \tag{7}$$

Summing these expressions, we obtain the aggregate growth rate $v = d_g/\delta t$. The dimensionless equations of the length as a function of the time during the accretion are:

$$\frac{d\zeta}{d\tau} = \frac{1}{1+\zeta/2}, \quad \text{and thus} \quad \zeta(\tau) = 2(\sqrt{1+\tau}-1). \tag{8}$$

These predictions are compared to our experimental measurements in Fig. 3. The smooth transition from the capture regime to the viscous regime is well captured by our model, which highlights the coupling between the fluid dynamics and the grains motion.

We now discuss the trapping mechanisms. The initial kinetic energy E_i of one impacting grain must be dissipated during the capture. Three main mechanisms have been identified. First, Crassous *et al.* have shown that the restitution coefficient of a grain bouncing on a dry granular pile ranges between 0.3 and 0.5 for our inclination (30° - 60°), which represents an energy loss from 75% to 90% of E_i [24]. Also, several works studied the capture of a grain by a flat liquid film [25–28], and showed the role of the viscous dissipation and the rupture distance of capillary bridges to predict the sticking condition. Here, based on a typical rupture distance $d_g/4$, the viscous and capillary energy dissipations are of the order of 5% and 10% of E_i [21]. Assuming that these three phenomena are independent, we conclude that the initial kinetic energy may be completely dissipated. However, the calculation of the probability $\mathcal{P}_0$ from the experimental value of v_0 indicates that only 2.5% of the grains are trapped at $\Delta h = 0$, which means that only 2.5% of the aggregate interface is able to capture a grain. This low efficiency can be explained by the crucial role of the position of the grain impact to fully dissipate the kinetic energy. If the liquid depth is too small, the grain will bounce off.

In conclusion, the flow of a dry granular material on a wet granular substrate induces an accretion process characterized by the growth of the saturated phase by the accretion of grains. We show that this capture is a local process controlled by the capture probability of grains, which is related to the liquid availability at the interface. The horizontal accretion process reveals two distinct regimes, depending on the mechanism that limits the presence of fluid at the surface of the aggregate, either the viscous displacement in the porous material or the hydrostatic depression. We propose a theoretical model that predicts the correct transition and dynamics. This study provides a solid grounding to understand the interaction between flowing granular media and a fluid flow.

We are grateful to William Woelffel for his help and his advice for the tomographic acquisitions and we acknowledge support from Saint-Gobain Recherche to access their lab tomograph. This work benefitted from the financial support of French ANRT (PhD. CIFRE 2015/0504).

[1] S. Herminghaus, Adv. Phys. **54**, 221 (2005).
[2] S. Nowak, A. Samadani, and A. Kudrolli, Nat. Phys. **1**, 50 (2005).
[3] P. C. F. Møller and D. Bonn, Europhys. Lett. **80**, 38002 (2007).
[4] C. Bonnoit, T. Darnige, E. Clement, and A. Lindner, J. Rheol. **54**, 65 (2010).
[5] F. Boyer, E. Guazzelli, and O. Pouliquen, Phys. Rev. Lett. **107**, 188301 (2011).
[6] T. G. Mason, A. J. Levine, D. Ertas, and T. C. Halsey, Phys. Rev. E **60**, R5044 (1999).
[7] C. D. Willett, M. J. Adams, S. A. Johnson, and J. P. K. Seville, Langmuir **16**, 9396 (2000).
[8] N. Mitarai and F. Nori, Adv. Phys. **55**, 1 (2006).
[9] A. Kudrolli, Nat. Mat. **7**, 174 (2008).
[10] M. Scheel, R. Seemann, M. Brinkmann, M. Di Michiel, A. Sheppard, B. Breidenbach, and S. Herminghaus, Nat. Mat. **7**, 189 (2008).
[11] S. M. Iveson, J. D. Litster, K. Hapgood, and B. J. Ennis, Powder Technol. **117**, 3 (2001).
[12] T. Delker, D. B. Pengra, and P. Z. Wong, Phys. Rev. Lett. **76**, 2902 (1996).
[13] M. Reyssat, L. Y. Sangne, E. A. van Nierop, and H. A. Stone, Europhys. Lett. **86**, 56002 (2009).
[14] J. Xiao, H. A. Stone, and D. Attinger, Langmuir **28**, 4208 (2012).
[15] J. Chopin and A. Kudrolli, Phys. Rev. Lett. **107**, 208304 (2011).
[16] B. Cazacliu and N. Roquet, Cem. Concr. Res. **39**, 182 (2009).
[17] G. Lefebvre and P. Jop, Phys. Rev. E **88**, 032205 (2013).
[18] G. Lefebvre, A. Merceron, and P. Jop, Phys. Rev. Lett. **116**, 068002 (2016).
[19] F. Pacheco-Vázquez, F. Moreau, N. Vandewalle, and S. Dorbolo, Phys. Rev. E **86**, 051303 (2012).
[20] P. S. Raux, H. Cockenpot, M. Ramaioli, D. Quéré, and C. Clanet, Langmuir **29**, 3636 (2013).
[21] See Supplemental Material at [url] for experimental methods and precisions, X-ray imaging methods, details of calculation and modelling, which includes Ref. [22].
[22] P. C. Carman, Trans. Inst. Chem. Eng. **15**, 150 (1937).
[23] E. W. Washburn, Phys. Rev. **17**, 273 (1921).
[24] J. Crassous, D. Beladjine, and A. Valance, Phys. Rev. Lett. **99**, 248001 (2007).
[25] R. H. Davis, D. A. Rager, and B. T. Good, J. Fluid Mech. **468**, 107 (2002).
[26] S. Antonyuk, S. Heinrich, J. Tomas, N. G. Deen, M. S. van Buijtenen, and J. A. M. Kuipers, Granular Matter **12**, 15 (2010).
[27] F. Gollwitzer, I. Rehberg, C. A. Kruelle, and K. Huang, Phys. Rev. E **86**, 011303 (2012).
[28] T. Müller and K. Huang, Phys. Rev. E **93**, 042904 (2016).

Supplemental Material

Guillaume Saingier, Alban Sauret, and Pierre Jop*
Surface du Verre et Interfaces, UMR 125, CNRS/Saint-Gobain,
39, quai Lucien Lefranc, F-93303 Aubervilliers, Cedex France

I. EXPERIMENTAL DETAILS

List of movies - Growth of an aggregate for different heights Δh. The flow rate of grains Q_g is equal to 1.1 g/s. The grains velocity at the impact on the wet aggregate v_g is about 1.6 m/s (measured by acquisitions with a high speed camera). Movies are accelerated 40 times. Scale bar is 2 cm.

- Movie 1a: $h_g = 10$ mm, $\Delta h = 5$ mm
- Movie 1b: $h_g = 10$ mm, $\Delta h = 35$ mm
- Movie 1c: $h_g = 10$ mm, $\Delta h = 62$ mm

Movie 2: Illustration of the evolution of the apparent liquid area at the surface of a wet granular material when increasing the hydrostatic depression (through the height Δh). Pictures are recorded with a binocular microscope. The wet granular material is composed of brown zirconium beads of 500 μm average diameter, the liquid used is milk.

Particle size distribution - Experiments were carried out with spherical glass beads from Marteau & Lemarié. The beads are sieved to reduce the grains polydispersity between 315 and 355 μm. The size distribution is calculated by a statistical measurement of grains sizes recorded by binocular microscopy and is plotted in Fig. S1(a).

Contact angle - The contact angle θ is measured by placing a single bead at the surface of the liquid. The contact angle is obtained from the distance $\delta = (d_g/2)\cos\theta$ between the center of the grain and the liquid interface (Fig. S1(b)) [1].

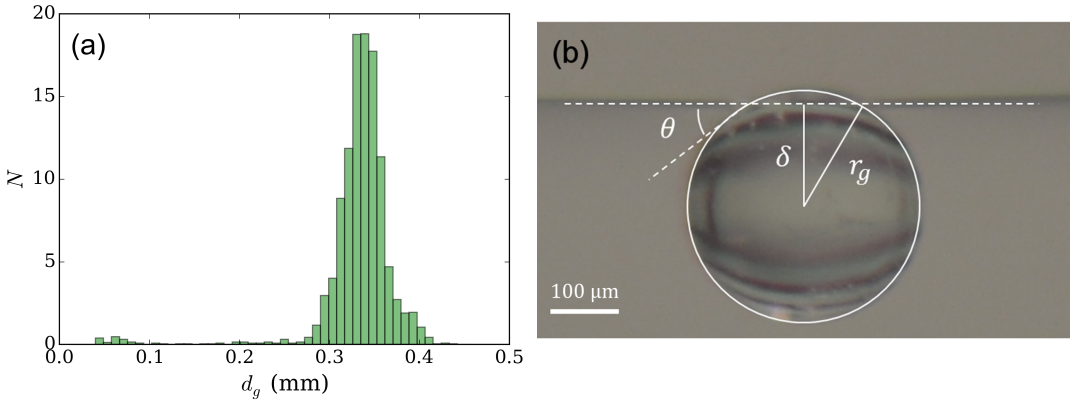

Figure S1. (a) Particle size distribution. (b) Picture of a glass bead at the air/water interface - $\theta = 27°$ ($\pm$ 5°).

II. INFLUENCE OF THE WETTABILITY OF THE SUBSTRATE

To ensure that the nature of the support does not influence the growth dynamics of the aggregate, we have performed experiments with a support whose wetting properties change along its length. By using a PTFE film (Teflon, θ =120° $\pm$ 5°), we have performed accretion growth experiments for two different values of Δh ($\Delta h = 10$ mm being in the

* pierre.jop@saint-gobain.com; http://svi.cnrs.fr/

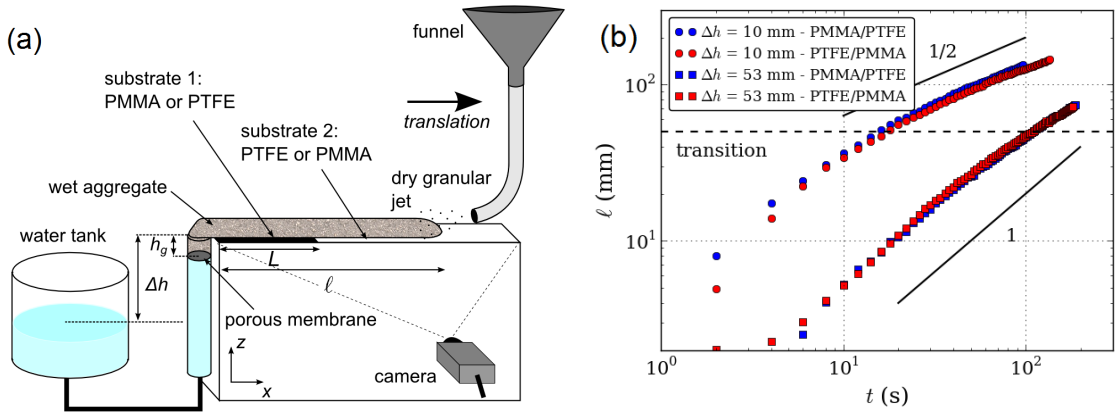

Figure S2. (a) Schematic of accretion experiment with different nature of support. (b) Growth dynamics for each support (PMMA/PTFE and PTFE/PMMA) for several Δh. Contact angle: PMMA $\theta = 70° \pm 5°$, PTFE $\theta = 120° \pm 5°$.

viscous regime and $\Delta h = 53$ mm being in the capture regime). The nature of the substrate changes after a length L = 5 cm [PMMA after PTFE and PTFE after PMMA, see Fig. S2(a)]. The results are presented on Fig. S2(b) and show that the growth dynamics is not modified by the change of the wettability of the substrate and the accretion dynamics is a robust phenomenon.

III. X-RAY TOMOGRAPHY IMAGING

We perform X-ray tomography experiments with a laboratory tomograph available at Saint-Gobain Research to investigate the microstructure of the aggregate. The X-ray radiations are generated by an electron gun bombing a tungsten plate, which produces photons at a peak energy of 40 keV. The spatial resolution is 7.5 μm and the detector fields of view is 13 mm x 10 mm. To increase the contrast between the different phases (grains, liquid and air), an aqueous zinc iodide solution at 0.5 g/mL is used as liquid to build the aggregate [2]. A tomographic acquisition consisted of 1395 projections, equally separated, is acquired in about 40 min and cover a total angle of 180°. The 3D reconstruction is performed from the set of 2D projections using a filtered backprojection algorithm.

A small aggregate is built by pouring a dilute granular jet on a substrate of 2 cm height of the same grains saturated by the aqueous solution. Then, the aggregate and the wet substrate, disconnected from the reservoir, are placed in a small closed container that is deposited in the tomograph for the acquisitions. A soaked tissue is placed in the cell to maintain a wet atmosphere and limits the evaporation. The mean compacity of the aggregate, found equal to $\phi = 0.63 \pm 0.01$, is measured using the tomographic reconstruction by binarizing pictures to separate the liquid, the grains and the air.

IV. LIQUID DISTRIBUTION AT THE INTERFACE

Calculation of the liquid surface fraction - In this section, we explain the calculation of the liquid distribution at the interface of the layer of monodispersed grains. The packing is hexagonal leading to compact layers. We note d_g the grain diameter and $S_T = 6\sqrt{3}(d_g/2)^2$ the surface of the unit hexagon drawn between the centers of 6 grains (Fig. S3a). The layer of grains is soaked by a wetting liquid (θ, γ, ρ). To simplify the geometric approximation, we assume that $\theta = 0$. At the air/liquid interface, the shape of the meniscus between 3 grains is assimilated to a portion of sphere of radius R (Fig. S3b). We calculate the minimal height of liquid h_{liq} by considering the right-angled triangle A_1GC between the center of a grain, the center of the circle described by the meniscus and the center of the triangle $A_1A_2A_3$ defined by the grains centers (see Fig. S3b)

$$(h_{liq} + R)^2 + \left(\frac{\sqrt{3}}{3} d_g\right)^2 = \left(R + \frac{d_g}{2}\right)^2, \tag{1}$$

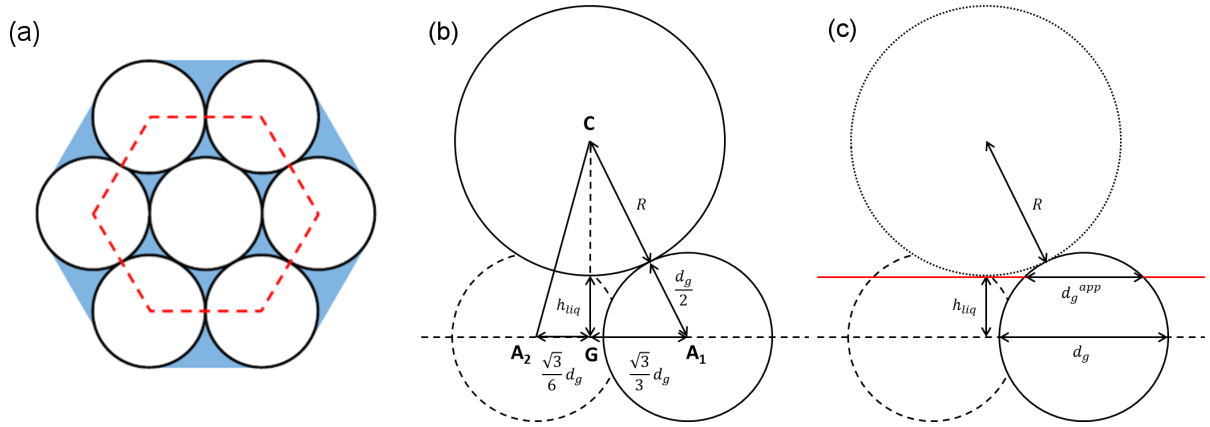

Figure S3. (a) Schematic of the top layer of monodispersed grains - top view. (b) Approximation of the shape of the meniscus between 3 grains as a portion of sphere - side view. (c) Approximation of the projected surface by neglecting the curvature of the meniscus.

which leads to

$$h_{liq} = R\sqrt{1 + \frac{d_g}{R} - \frac{1}{3}\left(\frac{d_g}{2R}\right)^2} - R. \tag{2}$$

To estimate the surface area of liquid and make the analytical calculation tractable, we neglect the curvature of the menisci and assume that their shape is described by a horizontal plan that intersects the grains at a height h_{liq}. Then, the apparent radius of immersed grains is defined as:

$$\frac{{d_g}^{app}}{2} = \sqrt{\left(\frac{d_g}{2}\right)^2 - {h_{liq}}^2}. \tag{3}$$

We note S^{app} the apparent surface occupied by the grains in the unit hexagon:

$$S^{app} = 3\pi\left(\frac{{d_g}^{app}}{2}\right)^2 \tag{4}$$

Finally, the surface fraction of liquid is defined as:

$$\phi_{liq} = \frac{S_{liq}}{S_T} = 1 - \frac{S^{app}}{S_T} = 1 - \frac{\pi}{2\sqrt{3}}\left(\frac{{d_g}^{app}}{d_g}\right)^2 \tag{5}$$

The surface fraction depends on the ratio between the radius of the grains and the radius of curvature $X = d_g/2R$. The pressure balance at the liquid/air interface leads to:

$$p_0 - \frac{2\gamma\cos\theta}{R} = p_0 - \rho g \Delta h, \tag{6}$$

the ratio X can be written as:

$$X = \left(\frac{d_g \rho g}{\gamma\cos\theta}\right)\Delta h. \tag{7}$$

The evolution of the theoretical liquid area ϕ_{liq} is plotted in Fig. 3(b) in the main article. It decreases with the dimensionless height X and is well fitted by an exponential expression:

$$\phi_{liq}(X) = \phi_\infty + (1 - \phi_\infty)\exp\left(-\frac{X}{{X_s}^\star}\right), \tag{8}$$

where ϕ_∞ is the surface porosity of the granular layer and ${X_s}^\star$ is the typical dimensionless length characterizing the decrease of the liquid area. The data fitting gives: $\phi_\infty = 0.11$ and ${X_s}^\star = 1.10$.

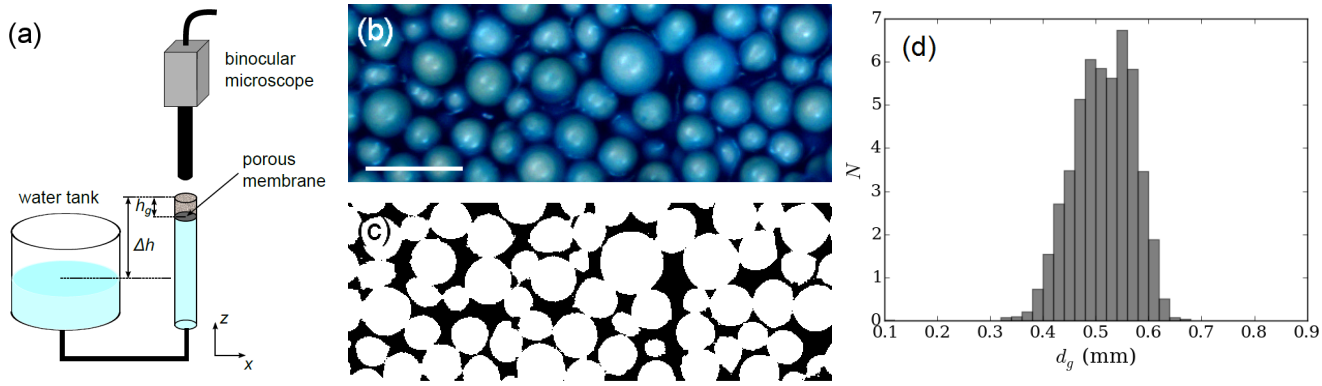

Figure S4. (a) Schematic of the set-up used to visualize the liquid repartition at the interface with air. (b) Pictures of the liquid area at the interface of a granular packing under depression ($\Delta h = 38.5$ mm). Scale bar is 2 mm. (c) Same picture after binarization of the green component to extract the liquid area. (d) Particle size distribution.

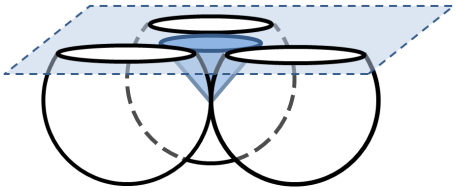

Figure S5. Schematic of the volume of a capture site between 3 grains by assimilating it to a cone.

Surface visualization - The repartition of the liquid at the interface was investigated experimentally by imaging the surface of a wet granular material with a binocular microscope. The hydrostatic depression is controlled by adjusting the liquid level as shown in Fig. S4. To make the binarization and the post processing easier, we used white zirconium beads ($d_g = 500$ μm) with dyed opaque liquid (milk + erioglaucine disodium). The surface tension and the contact angle of the liquid on the zirconium beads were measured: $\gamma = 44$ mN/m $\pm$ 2 mN/m - $\theta = 65° \pm 5°$. The experimental evolution of the liquid area at the surface of the granular packing is reported in Fig. 3(c) in the main article. The decrease of the measurements is well fitted by an exponential expression $\phi_{liq} = \phi_{\infty,exp} + (1 - \phi_{\infty,exp}) \exp(-X/{X_{s,exp}}^\star)$ with a characteristic dimensionless length ${X_{s,exp}}^\star = 1.59 \pm 0.26$ (uncertainty on the measurements) and a surface porosity $\phi_{\infty,exp} = 0.16$.

Variation of the volume of a capture site - We now consider that the capture efficiency could not only be associated to the apparent liquid availability at the interface but also to the liquid volume in some locations between grains. In this model, a grain can be trapped only if it falls in a well constituted by 3 grains. This liquid volume is approximated by a cone of radius r_{liq} and of depth h_{liq} inscribed between the grains as shown in Fig. S5. The cone radius is defined as:

$$r_{liq} + {r_g}^{app} = \frac{2\sqrt{3}}{3} r_g \quad \text{such that} \quad r_{liq} = \frac{2\sqrt{3}}{3} r_g - {r_g}^{app}. \tag{9}$$

The volume of the unit cone is:

$$V = \frac{1}{3} h_{liq} \pi {r_{liq}}^2. \tag{10}$$

The evolution of this volume with the hydrostatic depression can also be fitted by a exponential decrease characterized by a typical dimensionless length ${X_v}^\star = 0.34$, corresponding to ${h_v}^\star = 26$ mm for glass beads with water. This value is close to the characteristic length associated to the accretion process, indicating that the volume of fluid available for the capture is a critical parameter for the capture. Fitting parameters: $V = V_0 \exp(-X/{X_v}^\star)$ - ${X_v}^\star = 0.34$ - $V_0 = 0.26$.

Influence of the contact angle - Note that if the contact angle is increased, the qualitative results of the model hold but the values of the characteristic lengths $X^\star$ are shifted toward lower values.

V. ACCRETION PARAMETERS

The experimental measurements of the growth rates are rescaled by the time t_c and length ℓ_c, which characterize the accretion dynamics:

$$t_c = \frac{k}{2\eta}\Delta p \left(\frac{\rho_g \phi S}{P_{capt} Q_g}\right)^2, \quad \ell_c = \frac{k}{2\eta}\Delta p \frac{\rho_g \phi S}{P_{capt} Q_g}. \tag{11}$$

We take the following parameters for the rescaling that depend on the liquid and grains properties but also on the packing:

◦ water: $\gamma = 71$ mN/m, $\theta = 27°$, $\eta = 1$ mPa.s, $\rho = 1000$ kg/m^3.

◦ glass beads: $\rho_s = 2500$ kg/m^3, $\bar{d}_g = 340$ μm.

◦ granular packing: $\phi = 0.63$ (measured from the tomography reconstructions), $k = 7.96 \times 10^{-11}$ m^2, estimated with the Carman-Kozeny's formula [3]:

$$k = \frac{{d_g}^2}{180}\frac{\varepsilon^3}{(1-\varepsilon)^2}, \tag{12}$$

where $\varepsilon = 1 - \phi = 0.37$ is the porosity.

◦ capillary pressure $p_c = \gamma \cos\theta / d_g = 753$ Pa.

◦ sticking probability $P_{capt} = P_0 \exp(-\Delta h / h^\star)$ with $h^\star = 20$ mm, $P_0 = (\rho_g \phi S v_0)/Q_g$ and $v_0 = 1.86$ mm/s. Note that S, ρ_g and Q_g are not directly present in the equation but influence the value of v_0.

VI. ENERGY DISSIPATION AND STICKING CONDITION

In this section, we describe the mechanisms responsible for the grains capture at the interface of a wet aggregate. Considering a grain impacting the wet aggregate at a velocity v_g, the associated kinetic energy E_i is:

$$E_i = \frac{1}{2}\left(\frac{1}{6}\pi {d_g}^3\right)\rho_s {v_g}^2, \tag{13}$$

such that $E_i = 6.58 \times 10^{-8}$ J. Three mechanisms have been identified to dissipate this energy to capture the grain. The most important part of the dissipation is associated to the friction in the granular packing. In the case of the impact on a dry packing, the restitution coefficient, defined as the ratio between the velocity after impact and the velocity before impact, varies between 0.3 and 0.5 depending on the inclination of the surface at the impact [4]. Assuming that the parameters of the impact are the same in the wet and the dry cases, it represents an energy loss from 75 % to 90 % of the kinetic energy E_i. The remaining of the dissipation results from the liquid between the grains that can dissipate the energy by viscous and capillary effects. We assume that the fluid dissipation is similar to the case of a liquid layer on a solid surface to estimate the viscous dissipation. The viscous force acting on the particle is [5]:

$$F_{visc} = \frac{3\pi}{2}\eta {d_g}^2 \frac{v_g}{x}, \tag{14}$$

where x is the distance between the grain and the plate. Assuming that the same distance is traveled during the approach and the departure, equal to $d_g/4$, we obtain by summing over the distance [6]:

$$E_{visc} = 3\pi\eta {d_g}^2 v_g \ln\left(\frac{d_g}{4\epsilon}\right), \tag{15}$$

where $\epsilon = 5$ μm is the estimated roughness of the grain. It leads to $E_{visc} = 4.94 \times 10^{-9}$ J, which represents 7 % of the kinetic energy. The capillary dissipation corresponds to the deformation and the rupture of the liquid bridge and can be estimated by integrating the force arising from the surface tension over the stretching length. The capillary force between two grains is given by [6, 7]:

$$F_{cap} = \frac{\pi d_g \gamma \cos\theta}{1 + 2.1 S^\star + 10 {S^\star}^2} \tag{16}$$

where $S^\star = s\sqrt{d_g/2V_b}$ is the half of the separation distance s rescaled by a characteristic length, which depends on the bridge volume V_b. By integrating until a rupture length equal to $d_g/4$, an estimation of the rupture energy is:

$$E_{cap} \simeq \pi\gamma\cos\theta\sqrt{2V_b d_g}, \tag{17}$$

where V_b is approximated by $V_b \simeq {d_g}^3/16$. With these assumptions, the capillary dissipation is $E_{cap} = 7.78 \times 10^{-9}$ J, that represents 12 % of the kinetic energy E_i.

---

[1] P. Raux, H. Cockenpot, M. Ramaioli, D. Quéré & C. Clanet, Langmuir **29**, 11, 3636 (2013).
[2] M. Scheel, R. Seeman, M. Brinkman, M. di Michel, A. Sheppard, B. Breidenbach & S. Herminghaus, Nat. Mater. **7**, 189 (2008).
[3] P. C. Carman, Trans. Inst. Chem. Eng. **15**, 150 (1937).
[4] J. Crassous, D. Beladjine, and A. Valance, Phys. Rev. Lett. **99**, 248001 (2007).
[5] R. H. Davis, D. A. Rager, and B. T. Good, J. Fluid Mech. **468**, 107 (2002).
[6] F. Gollwitzer, I. Rehberg, C. A. Kruelle, and K. Huang, Phys. Rev. E **86**, 011303 (2012).
[7] C. D. Willett, M. J. Adams, S. A. Johnson, and J. P. K. Seville, Langmuir **16**, 9396 (2000).